Society For Biomaterials

Effects of calcium phosphate composition in sputter coatings on *in vitro* and *in vivo* performance

Eva R. Urquia Edreira,[1] Joop G. C. Wolke,[1] Abdullah AlFarraj Aldosari,[2,3] Sulieman S. Al-Johany,[2,3] Sukumaran Anil,[3,4] John A. Jansen,[1,3] Jeroen J. J. P. van den Beucken[1]

[1]Department of Biomaterials, Radboudumc, PO Box 9101, 6500 HB Nijmegen, The Netherlands
[2]Department of Prosthetic Dental Science, College of Dentistry, King Saud University, Riyadh, Saudi Arabia
[3]Dental Implant and Osseointegration Research Chair (DIORC), College of Dentistry, King Saud University, Riyadh, Saudi Arabia
[4]Department of Periodontics and Community Dentistry, College of Dentistry, King Saud University, Riyadh, Saudi Arabia

Received 12 March 2014; accepted 17 March 2014
Published online 3 April 2014 in Wiley Online Library (wileyonlinelibrary.com). DOI: 10.1002/jbm.a.35173

Abstract: Calcium phosphate (CaP) ceramic coatings have been used to enhance the biocompatibility and osteoconductive properties of metallic implants. The chemical composition of these ceramic coatings is an important parameter, which can influence the final bone performance of the implant. In this study, the effect of phase composition of CaP-sputtered coatings was investigated on *in vitro* dissolution behavior and *in vivo* bone response. Coatings were prepared by a radio frequency (RF) magnetron sputtering technique; three types of CaP target materials were used to obtain coatings with different stoichiometry and calcium to phosphate ratios (hydroxyapatite (HA), α-tricalciumphosphate (α-TCP), and tetracalciumphosphate (TTCP)) were compared with non-coated titanium controls. The applied ceramic coatings were characterized by X-ray diffraction, Fourier transform infrared spectroscopy, scanning electron microscopy, and inductively coupled plasma optical emission spectroscopy. The *in vitro* dissolution/precipitation of the CaP coatings was evaluated using immersion tests in simulated body fluid (SBF). To mimic the *in vivo* situation, identical CaP coatings were also evaluated in a femoral condyle rabbit model. TCPH and TTCPH showed morphological changes during 4-week immersion in SBF. The results of bone implant contact (BIC) and peri-implant bone volume (BV) showed a similar response for all experimental coatings. An apparent increase in tartrate resistant acid phosphatase (TRAP) positive staining was observed in the peri-implant region with decreasing coating stability. In conclusion, the experimental groups showed different coating properties when tested *in vitro* and an apparent increase in bone remodeling with increasing coating dissolution *in vivo*. © 2014 Wiley Periodicals, Inc. J Biomed Mater Res Part A: 103A: 300–310, 2015.

Key Words: RF magnetron sputtering, calcium phosphate coatings, simulated body fluid (SBF), Ca/P ratio, bone healing

How to cite this article: Urquia Edreira ER, Wolke JGC, Aldosari AA, Al-Johany SS, Anil S, Jansen JA, van den Beucken JJJP. 2015. Effects of calcium phosphate composition in sputter coatings on *in vitro* and *in vivo* performance. J Biomed Mater Res Part A 2015:103A:300–310.

INTRODUCTION

Calcium phosphate (CaP) based ceramics are commonly used synthetic materials for bone substitutes and bone implant surface modification.[1] Properties including biodegradability, bioactivity, osteoconductivity, and osteoinductivity make calcium phosphates biologically appealing implant materials.[2,3] Differences in dissolution behavior of bulk ceramics are due to changes in chemical composition (CaP phase) and have been associated with osteoinductive potential *in vivo*.[4] More specifically, hydroxyapatite (HA), tricalcium phosphate (TCP), and biphasic calcium phosphate (BCP) have shown different levels of osteoinductive capacity that inversely correspond to their biological stability (i.e., TCP > BCP > HA).[4] However, because of the inferior mechanical properties of bulk CaP ceramics, their application under load-bearing conditions is limited. Under load-bearing conditions, CaP ceramics are used as coating on mechanically strong bioinert implant materials, such as titanium (or titanium alloy), for optimization of the interaction with bone tissue at the interface.[5]

Compared with bulk ceramics, as-deposited coatings possess distinctive network structures and properties (i.e., surface roughness, coating thickness, and crystallinity) and therefore can evoke a different response *in vivo*. The most commonly investigated synthetic CaP ceramic materials for use as coatings are HA ($Ca_{10}(PO_4)_6OH_2$)[6–8] and TCP ($Ca_3(PO_4)_2$).[9,10] These CaP-based ceramics differ in composition, crystal structure, and resorption rate. HA resorbs

Correspondence to: J. A. Jansen; e-mail: john.jansen@radboudumc.nl
Contract grant sponsors: BioMedical Materials Institute, Dutch Ministry of Economic Affairs, Agriculture and Innovation (Project P2.04 BONE-IP)

slowly and resembles more closely natural bone mineral than TCP.[11] Therefore, HA is more commonly used for medical application. Among CaP-based ceramics, tetracalcium phosphate (TTCP; $CaO.Ca_3(PO_4)_2$) has the highest solubility at $pH < 4.0$ and is the only CaP ceramic with a Ca/P ratio greater than HA.[12] TTCP is formed only by a solid-state reaction above 1300°C and in aqueous solutions complete hydrolysis of TTCP to HA occurs. However, very little research has been done on the use of TTCP as a CaP coating[13,14] and, to our knowledge, no attempts have been made to evaluate the performance of either TCP and TTCP sputtered coatings *in vivo*. Nevertheless, this seems to be interesting due to the suggested osteoinductive potential of the various CaP phases.[4]

Plasma spraying of CaP ceramics onto metallic implants has been commonly used for biomedical applications, despite poor control of thickness, and surface morphology.[15–17] However, radio frequency (RF) magnetron sputtering has several advantages over plasma spraying of CaP such as deposition of dense, uniform, and continuous coatings that have high CaP coating-substrate bonding strength.[18] After sputtering onto a metallic implant, the stoichiometry, CaP ratio, crystallinity, phase composition, and structure of the CaP ceramic are different relative to the bulk material. As a final step, post-annealing treatment is necessary to crystallize the coating, which also influences the final coating properties.[19] The resultant coating properties might enhance implant fixation and the bone formation processes.

The aim of this study was to evaluate the effect of CaP-sputtered coatings with different phase composition on (i) *in vitro* dissolution, and (ii) *in vivo* bone response. For this purpose, three different CaP-based target materials (i.e. HA, TCP, and TTCP) were used for coating preparation, after which coating characterization, *in vitro* dissolution experiments, and *in vivo* implantation in a rabbit femoral condyle model (6 weeks implantation) were performed. We hypothesized that different CaP-based target materials affect coating properties and lead to coating-specific dissolution/precipitation behavior *in vitro* and bone response *in vivo*.

MATERIALS AND METHODS

Materials

Commercially available pure Ti discs (thickness 1.5 mm, diameter 12 mm) and cylindrical Ti implants (length 8 mm, diameter 3.25 mm) were Al_2O_3 grit-blasted before deposition. The target materials used in the deposition process were HA granulated powder obtained from CAMCERAM® (CAM Bioceramics, Leiden, The Netherlands) and a copper disc provided with either a plasma-sprayed α-TCP or TTCP coating (CAM Bioceramics, Leiden, The Netherlands). The chemical composition and purity of the different target materials was confirmed by X-ray diffraction (XRD).

Coating deposition and characterization

The coatings for this study were deposited using RF magnetron sputtering equipment (Edwards High Vacuum ESM 100 system, Crawford, England).[18,20,21] Substrates were cleaned ultrasonically in acetone and ethanol before deposition to remove impurities. Subsequently, substrates were placed on a rotating holder. The distance between target and implants was 80 mm. During deposition, argon pressure was kept at 5×10^{-3} mbar and a sputter power of 400 W with a coating thickness of 1 μm was used. A non-coated implant was used as control for the experiments.

After deposition, all coatings were subjected to an additional heat-treatment of 15 s in air at final heating temperature of up to 650°C in an infrared furnace (Quad Ellipse Chamber, Model E4- 10-P, Research, MN).[22] The following ceramic coatings were generated:

1. HAH → Coating deposited using HA as target material + HT
2. TCPH → Coating deposited using α-TCP as target material + HT
3. TTCPH → Coating deposited using TTCP as target material + HT

CaP-coated substrates were characterized using scanning electron microscopy (SEM, Jeol, SEM6310, Tokyo, Japan), reflection Fourier-transform infrared spectroscopy (FTIR, Perkin Elmer, Spectrum One, Groningen, The Netherlands) and thin-film X-ray diffraction (XRD, Philips, PW3710, Eindhoven, The Netherlands). To determine the Ca/P molar ratio, the coatings were dissolved in concentrated nitric acid. After digestion, the samples were diluted to 5 mL of 1% HNO_3 and the solution was analyzed by inductively coupled plasma optical emission spectroscopy (ICP-OES, iCAP 6000 Thermo Fischer Scientific) for Ca and P ions.

In vitro evaluation

The *in vitro* dissolution of the CaP-based coatings was evaluated in conventional SBF with an ionic composition almost equal to human plasma.[23] Ionic concentrations of the SBF were 142.0 m*M* Na^+, 5.0 m*M* K^+, 1.5 m*M* Mg^{2+}, 2.5 m*M* Ca^{2+}, 147.8 m*M* Cl^-, 4.2 m*M* HCO_3^{-2}, 1.0 m*M* HPO_4^-, and 0.5 m*M* SO_4^{-2}. Tris-HCl served as a buffer to maintain a constant pH value of 7.4. The coated and uncoated discs (three specimens per time period per type of CaP coating) were immersed in 4 mL of SBF for 1, 2, and 4 weeks. In total, 36 CaP-coated discs were immersed in SBF ($n = 3$ for HAH, TCPH, TTCPH and uncoated Ti-discs). SBF temperature was maintained at 37°C and the solution was refreshed weekly. At each time point, the discs were removed from the SBF, washed with distilled water and dried at room temperature. Subsequently, all discs were characterized using XRD, FTIR, ICP-OES, and SEM.

In vivo experiment

Animals and regulations. The research protocol for animal experimental procedures was approved by the ethical committee of King Saud University (Riyadh, Kingdom of Saudi Arabia), and national guidelines for care and use of laboratory animals were observed. A total of 20 New Zealand

white rabbits (female; 6 months old) weighing between 3.2 and 5.1 kg were used.

Surgical procedure. Surgery was performed under general anesthesia by intramuscular injections of a combination of a dose of 35 mg/kg ketamine and a dose of 5 mg/kg xylazine. The rabbits were immobilized on their back and the hind limbs were shaved, washed and disinfected with povidone-iodine. The left and right femoral condyles were then exposed to a medial longitudinal incision. A hole (3.2 mm in diameter and 8 mm in depth) was created in the center of the condyle using a dental drill (KAVO, Intrasept 905, KAVO Nederland BV, Vianen, the Netherlands). A 2 mm drill bit was first used to establish a 2 mm diameter defect. The bone defect was gradually widened to a final diameter of 3.2 mm. Debris was removed from the defect by irrigation with physiological saline solution. The implants were placed into the defects. Subsequently, the periosteum and muscle were closed with a continuous 4-0 Vicryl suture. Finally, the skin was closed with continuous intracutaneous 4-0 Vicryl sutures. Post-surgery pain was controlled for two days postperatively by the administration of Fynadyne® (Fynadine, Schering Plough Animal Health Benelux, Utrecht, The Netherlands) intramuscularly. To reduce the post-operative infection risk Enrofloxacin 5–10 mg/kg (Baytril, Bayvet Division, Chemagro Ltd, Etobicoke, Ontario; 5–10 mg/kg) was administered. The implants were randomized according to a balanced split plot design to exclude the effect of implantation location and possible variations in individual rabbits. Each rabbit received two implants, in total 40 implants were placed ($n = 10$ for HAH, TCPH, TTCPH, and uncoated implants). Rabbits were euthanized 6 weeks after implantation and the femoral condyles were harvested and fixed in 10% formaldehyde solution, and dehydrated in ethanol for evaluation.

Micro-computed tomography. For micro-computed tomography, harvested femoral condyles were wrapped in parafilm® to prevent drying. For quantitative 3D analysis, all specimens were vertically placed onto the sample holder, with the long axis of the implant perpendicular to the scanning beam, and scanned using Skyscan-1072 X-ray microtomograph, TomoNT version 3N.5, Skyscan®, Belgium. Subsequently, a high resolution scan was recorded at a 30 μm voxel resolution. Then, using CT Analyzer (version 1.4, Skyscan®), a cone beam reconstruction was performed onto the projected files. The region of interest (ROI) was specified for distinct areas starting at the implant surface: inner (0–300 μm), middle (300–600 μm), and outer (600–900 μm) surrounding the implant over a constant length (4 mm). Thereafter, for all images a threshold was manually selected to discriminatively assign bone tissue and preserve its morphology, while excluding the metallic implant material. Per implant, the parameters of bone volume and tissue volume were measured, after which the amount of bone volume per zone was determined and expressed as a percentage.

Histological processing and analysis. Each specimen was hemisected along the longitudinal axis of the implant with a diamond saw blade. Subsequently, one half containing the implant was fixed in 4% formaldehyde for 2 days, dehydrated in increasing ethanol concentrations (70%–100%) and embedded in methylmethacrylate (MMA). After polymerization in MMA, thin sections (10 μm) were sawed in a longitudinal direction to the axes using a modified sawing microtome technique.[24] MMA sections were stained with methylene blue/basic fuchsine, basic fuchsine was used to color mineralized and unmineralized bone tissue (i.e., osteoid).[25] Implants from the second half of the specimens were carefully removed from the bone tissue to avoid interface damage. Afterward, the specimens were decalcified with a specific-purpose apparatus (TDE30, Sakura; Sakura Finetek Europe B.V. Alphen aan den Rijn, The Netherlands) for 3 weeks, dehydrated through a graded series of ethanol, embedded in paraffin and cut into sections along the longitudinal axis of the implant. Using a microtome (Leica RM 2145), 5 μm thick sections were prepared and stained using elastica-van Gieson (EVG), Masson-Goldner, and tartrate-resistant acid phosphatase. All sections were examined with a light microscope (Leica Microsystems AG, Wetzlar, Germany).

Histomorphometrical analysis. To evaluate the peri-implant bone response, histomorphometrical analyses were performed using a computer-based image analysis technique (Leica® Qwin Pro-image analysis system, Wetzlar, Germany). Sections of MMA-embedded specimens ($n = 3$ per specimen) were quantitatively analyzed for the percentage of bone-to-implant contact (BIC) and peri-implant bone volume (BV). BIC was defined as the relative implant surface distance at which direct bone-to-implant contact was present. To determine the peri-implant BV, three zones surrounding the implant were defined starting at the implant surface, that is, inner 0–300 μm, middle 300–600 μm, and outer 600–900 μm over a length of 4 mm. Consecutive elastic-van Gieson stained sections were used to verify assignment of tissue as bone tissue in the ROI.

In addition, Masson-Goldner stained sections were analyzed ($n = 3$ per specimen) to specifically determine the presence of unmineralized bone matrix (i.e., osteoids) in contact with the implant surface. To determine the presence of osteoclast-like cells in a peri-implant region of 900 μm (over 4 mm implant length) tartrate-resistant acid phosphatase (TRAP) staining was used. Results are presented as a percentage of TRAP-positive stained sections of the total number of sections analyzed.

Statistical analysis. All statistical analyses were performed with GraphPad Instat® 3.05 software (GraphPad Software, San Diego, CA), using analysis of variance (ANOVA) combined with a *post hoc* Tukey-Kramer Multiple Comparisons Test. Results were considered significant at $p < 0.05$. Chi-square test was applied to assess the presence of TRAP-positive staining.

RESULTS

Characterization and *in vitro* evaluation

Ca and P and the Ca/P ratio were determined by ICP-OES (Table I). This analysis revealed that all the as-sputtered

TABLE I. Nomenclature, Chemical Formula, and Ca/P Ratio of CaP-Based Ceramics

Nomenclature	Chemical Formula	Abbreviation	Ca/P Ratio[a]	Ca/P Ratio After HT[b]
Hydroxyapatite	$Ca_{10}(PO_4)_6(OH)_2$	HA	1.67	2.07 ± 0.01
α-Tricalcium phosphate	$Ca_3(PO_4)_2$	TCP	1.5	2.17 ± 0.01
Tetracalcium phosphate	$CaO{\cdot}Ca_3(PO_4)_2$	TTCP	2.0	2.30 ± 0.01

[a]Theoretical Ca/P ratio.
[b]Experimentally determined Ca/P ratio by ICP-OES after coating deposition + heat treatment (HT).

and heat-treated coatings had a higher Ca/P ratio compared with the theoretical value of the initial target materials. The Ca/P ratio for HAH, TCPH and TCPH coating was in the range of 2.07, 2.17, and 2.30, respectively.

Figure 1 shows the XRD patterns of the sputtered coatings before, during and after 4 weeks incubation in SBF. The XRD patterns of the as-sputtered coatings showed an amorphous structure without specific reflection lines (data not shown). Heat treatment at 650°C changed the amorphous structure into a more random apatite structure with peaks at 25.9°, 31.9°, and 32.4° 2θ (Fig. 1, lower lines). The XRD-patterns of the HAH coating did not show any change during the 4 week incubation period [Fig. 1(A)]. Typical reflection peaks at 25.9°, 31.7°, 32.0°, and 34.0° 2θ were attributed to the apatite phase. After 4 weeks incubation, the XRD patterns of the TCPH [Fig. 1(B)] and TTCPH coatings [Fig. 1(C)] showed an increase in crystallinity with more intense CaP diffraction peaks.

The phase composition was confirmed by the FTIR analysis. HAH coating showed bands at 1090, 1050, 970, 670, and 575 cm^{-1}, which were assigned as the stretching and bending motion of phosphate characteristics for hydroxyapatite [Fig. 2(A)]. These P—O bonds remained present and unchanged throughout the four weeks incubation in SBF. For the spectrum of the TCPH and TTCPH coatings [Fig. 2(B,C)], the bands present at 1090, 1050, 670, and 575 cm^{-1} split up into sharper bands. Furthermore, carbonate apatite (CO_3-AP) bands became apparent at wavelengths of 1454 and 1404 cm^{-1} with increasing incubation time, revealing that carbonate was mainly substituting for phosphate anions in a crystalline CaP environment.

Scanning electron micrographs of the heat-treated and SBF incubated coatings are shown in Figure 3. SEM examination of the heat-treated coatings showed a homogeneous layer and a complete coverage of the substrate surface. After two weeks incubation in SBF, TCPH, and TTCPH coatings showed morphological changes. For both coatings, local surface dissolution was observed, precipitates formed, and in the case of TTCPH coating the precipitate had a rod-like morphology (Fig. 3, higher magnification). This heterogeneous morphological appearance for TCPH and TTCPH coatings was maintained up to 4 weeks incubation. On the other hand, HAH coatings did not show any morphological changes during the 4 weeks incubation in SBF.

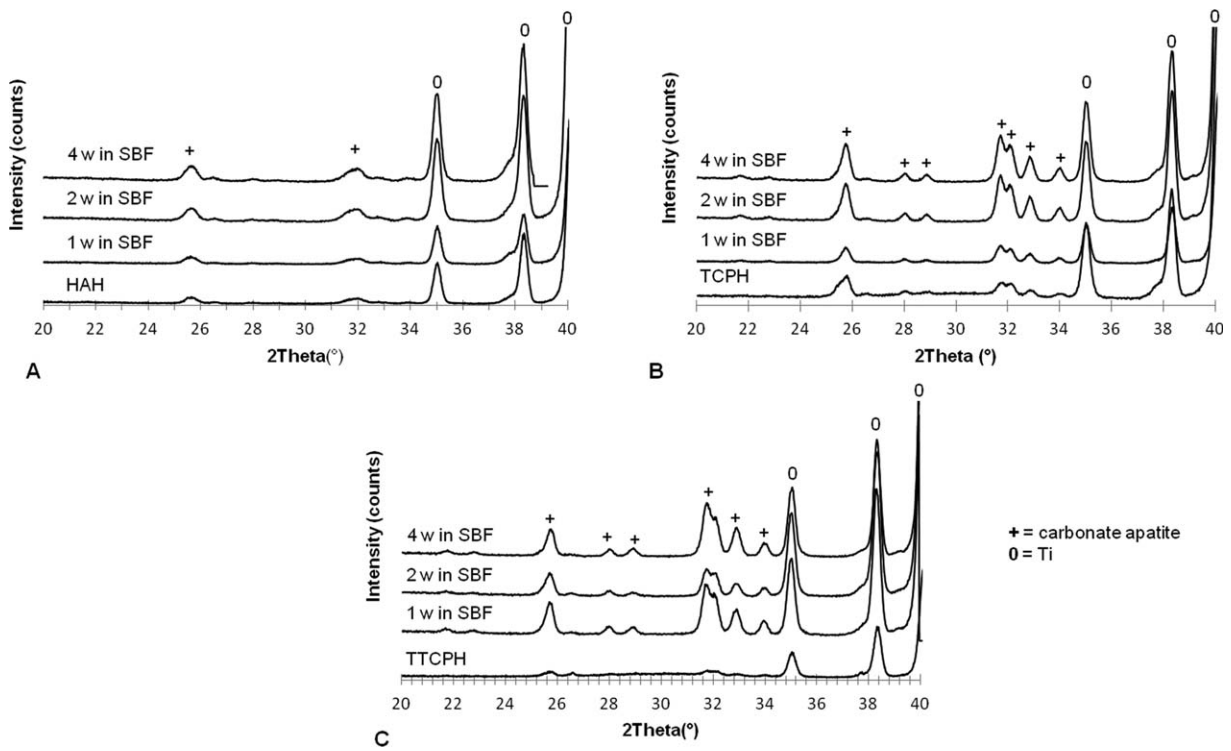

FIGURE 1. XRD pattern of HAH (A), TCPH (B), and TTCPH (C) coatings after 0, 1, 2, and 4 weeks of immersion in SBF.

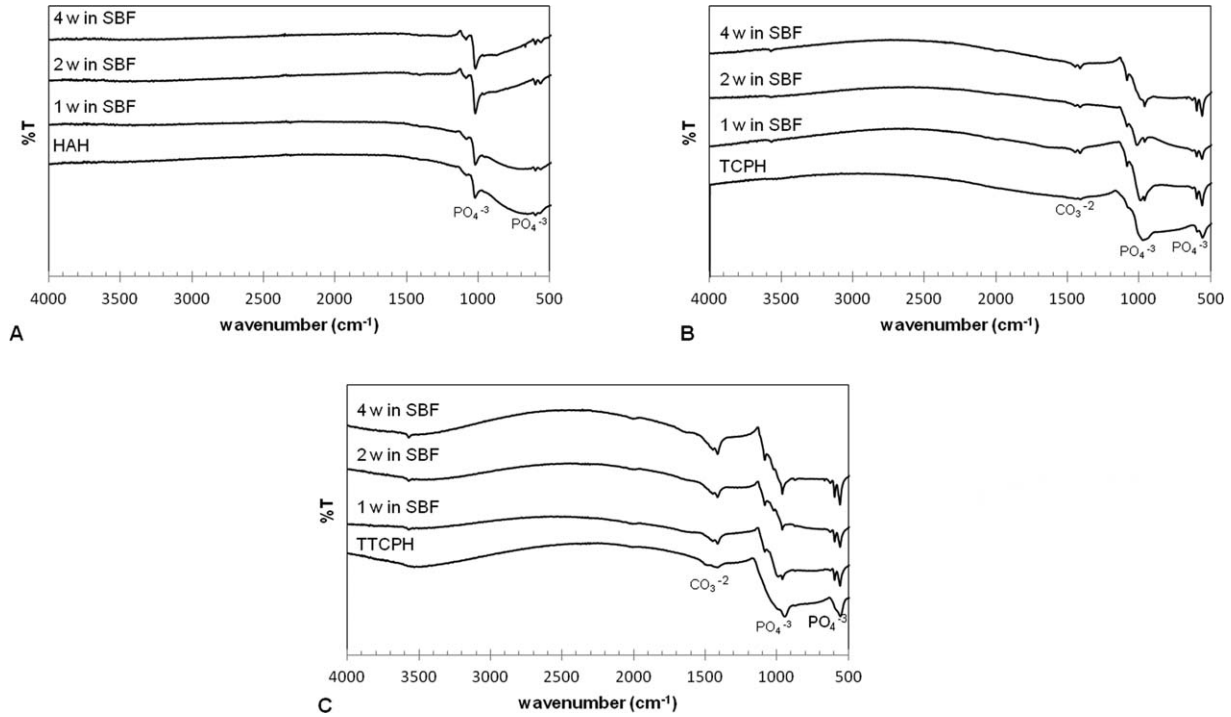

FIGURE 2. Fourier transform infrared of HAH (A), TCPH (B), and TTCPH (C) coatings after 0, 1, 2, and 4 weeks of immersion in SBF.

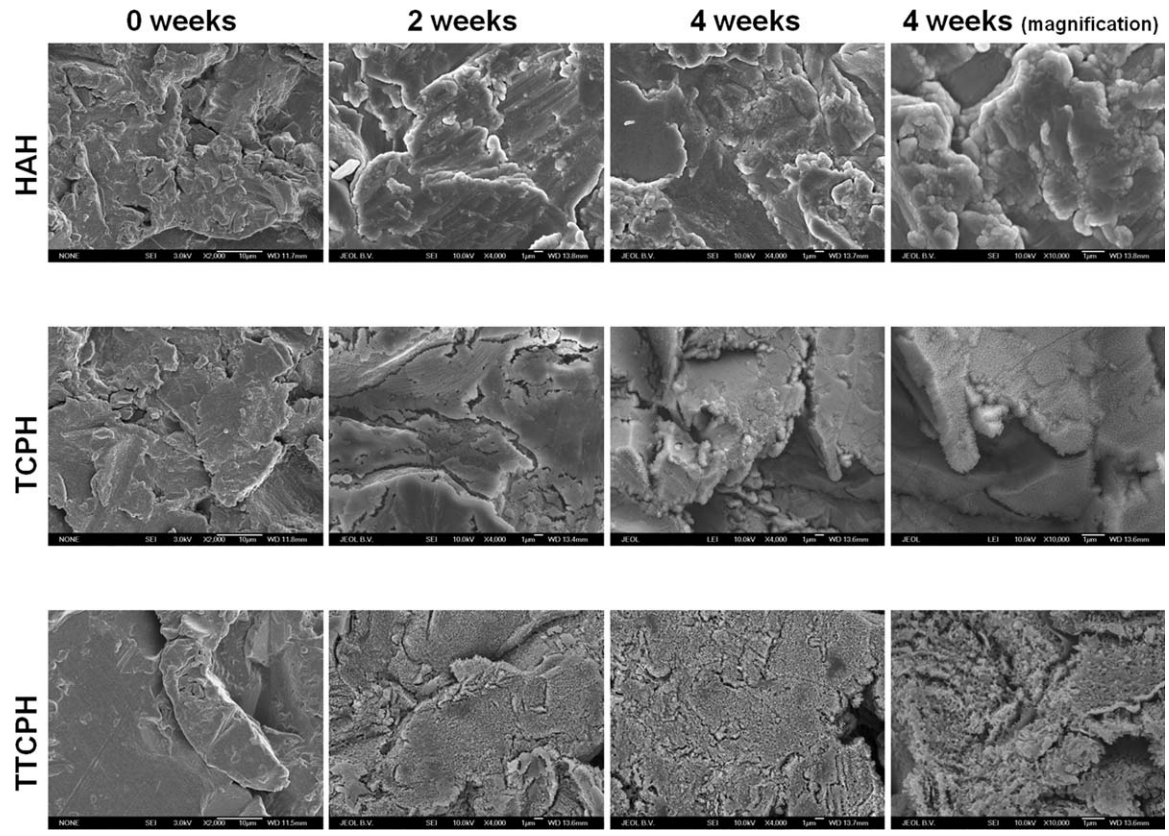

FIGURE 3. Scanning electron micrographs of HAH, TCPH, and TTCPH coatings after immersion in SBF for 0 (magnification 1000×), 2, and 4 weeks (magnification 4000×). Right panels show higher magnifications (10,000×) of the 4 week specimens.

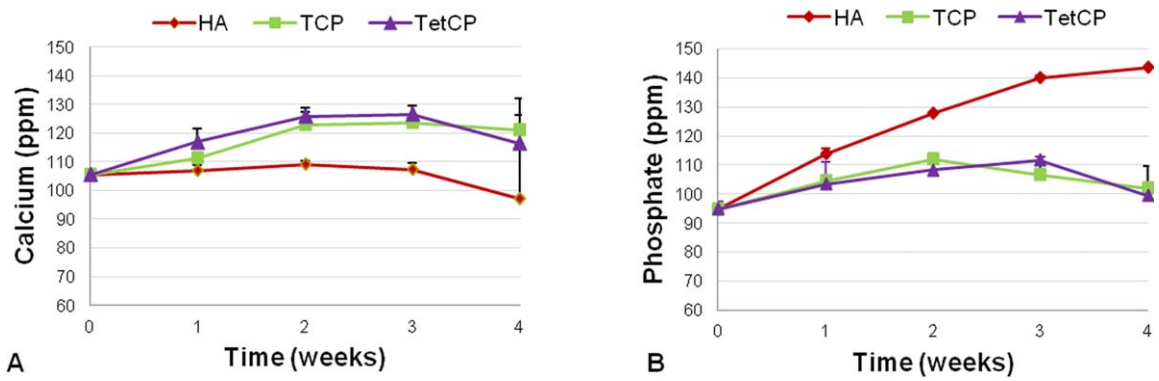

FIGURE 4. Calcium and phosphate ion concentration of the SBF solution during the 4-weeks incubation period of the different experimental coatings. [Color figure can be viewed in the online issue, which is available at wileyonlinelibrary.com.]

Changes in the concentration of calcium (Ca^{+}) and phosphate (PO_4^{3-}) ions in SBF of the CaP coatings during the 4-week incubation period are shown in Figure 4. HAH coating had stable Ca^{+} ion concentrations during the first 3 weeks of incubation, after which the concentration of Ca^{+} ions in SBF decreased. For the TCPH and TTCPH coatings, Ca^{+} ion concentration increased over the first 2 weeks of incubation with a subsequent stabilizing Ca^{+} ion concentration. HAH coatings showed an increase of PO_4^{3-} ion concentration during the 4-week incubation. TCP coatings showed an increase of PO_4^{3-} ion concentration during the first 2 weeks, after which the concentration in SBF solution decreased. TTCPH showed an increase of PO_4^{3-} ion concentration during the first 3 weeks, after which the concentration decreased.

General observations of *in vivo* implantation

All 20 animals remained in good health and did not show any wound healing complications. At the end of the implantation period, a total of 40 implants were harvested. At retrieval, no signs of inflammatory or adverse tissue reaction were observed around the implants. Post-mortem radiographs as obtained via micro-CT imaging revealed that the implants were located in trabecular bone [Fig. 5(A–C)].

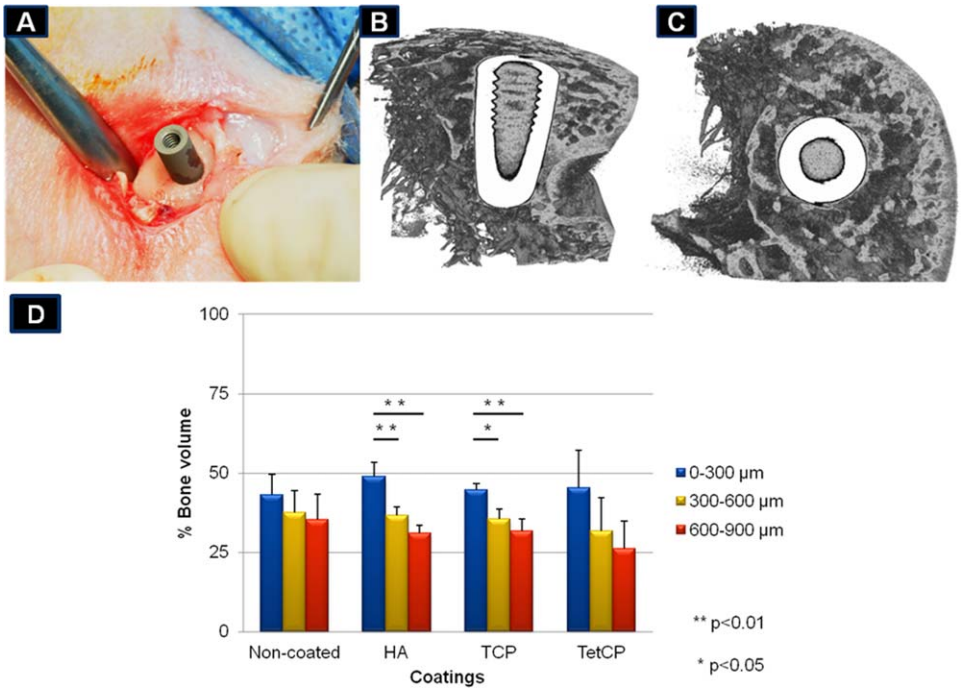

FIGURE 5. A: Surgical procedure of the titanium cylinder inserted in the femoral condyle of a rabbit. Post-sacrifice radiographs obtained with micro-computer tomography showing that the implants (i.e., metallic structures appear white) were mainly located in trabecular bone. B: cross-sectional view. C: top view of the implant. D: Results of micro-computed tomography (microCT) analysis of peri-implant BV percentage for the different experimental implants (non-coated, HAH, TCPH and TTCPH) in three different zones: inner (0–300 μm), middle (300–600 μm), and outer (600–900 μm). *$p<0.05$ and **$p<0.01$. [Color figure can be viewed in the online issue, which is available at wileyonlinelibrary.com.]

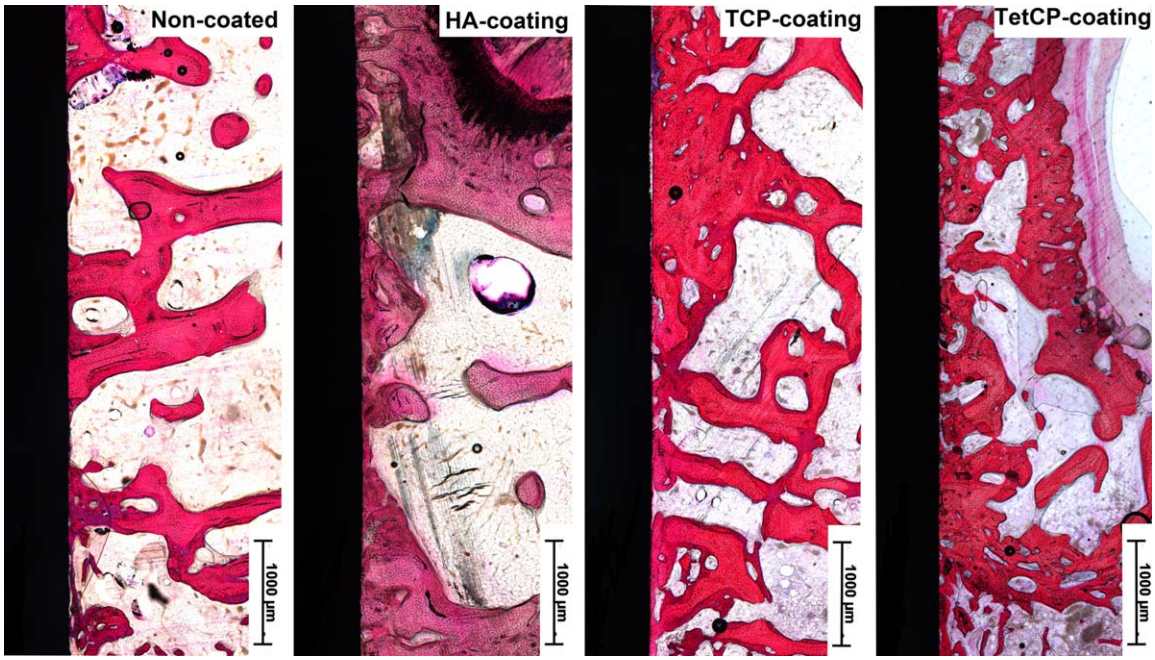

FIGURE 6. Representative histological sections (methylene blue/basic fuchsin stain) of the different experimental implants (non-coated, HAH, TCPH, and TTCPH) after 6 weeks of implantation in the femoral condyle of rabbits. [Color figure can be viewed in the online issue, which is available at wileyonlinelibrary.com.]

Micro-CT analysis

Peri-implant BV measurements were performed for three different regions of interest: 0–300 μm (inner), 300–600 μm (middle), and 600–900 μm (outer). Mean BV of the inner, middle, and outer zone are depicted in Figure 5(D). As a general trend, the highest BV (range: 43%–49%) was observed in the inner zone, intermediate BV (range: 31%–37%) in the middle zone and the lowest BV (range: 26%–35%) in the outer zone. Additionally, statistical analyses showed significant differences in BV for the inner zone compared with the middle (12.2%, $p < 0.01$) and outer zone (17.7%, $p < 0.01$) for HAH coatings and for the inner zone compared with the middle (9.2%, $p < 0.05$) and outer zone (13%, $p < 0.01$) for the TCPH coatings.

Descriptive histological evaluation

Histological examination was performed to evaluate the peri-implant bone response using MMA-embedded and paraffin-embedded sections.

MMA-embedded specimens stained with methylene blue/basic fuchsin (MB/BF) showed no indications of an inflammatory response at the implant interface. MMA-embedded specimens showed new bone formation around and bone apposition to all experimental implants. The non-coated implants had apparently less new bone formation around the implant than the HAH, TCPH and TTCPH coated implants (Fig. 6).

Results from Elastica-van Gieson (EVG) staining performed on the paraffin embedded specimens showed bone formation and bone apposition around all coated implants [Fig. 7(A)]. Masson-Goldner staining showed presence of immature new bone tissue (osteoid; unmineralized; red staining) as well as mineralized bone tissue (blue staining) at all the implant-tissue interface [Fig. 7(B)]. Furthermore, specimens displaying TRAP-positive staining contained osteoclast-like cells mainly close to the interface region of the implants [Fig. 7(C)].

Histomorphometry

BIC data for the different experimental groups are shown in Figure 8(A). The results of BIC measurements showed a similar response (values range: 60%–69%) for all experimental coatings.

Peri-implant BV was measured for distinct zones in the peri-implant region [Fig. 8(B)]. Significantly higher peri-implant BV was observed in the vicinity of the implant surface of the inner zone 0–300 μm compared with middle 300–600 μm for the HAH coating (difference 16.6%, $p < 0.05$) and TTCPH coating (difference 13%, $p < 0.05$). Further, similar peri-implant BV were found between the groups for individual zones in the peri-implant region ($p > 0.05$).

Osteoid-implant contact values were within a range of 38%–46% without significant differences between the experimental implants [Fig. 8(C)]. TRAP-positive staining was present in 17% of the sections of non-coated, 40% of the sections of HAH, 60% of the sections of TCPH, 75% of the sections of TTCPH coated implants (Table II). Although a higher percentage of TRAP-positive staining was found in coated than non-coated specimens, no statistical differences were found ($p > 0.05$).

DISCUSSION

The aim of this study was to evaluate the effect of phase composition of different CaP-sputtered coatings prepared

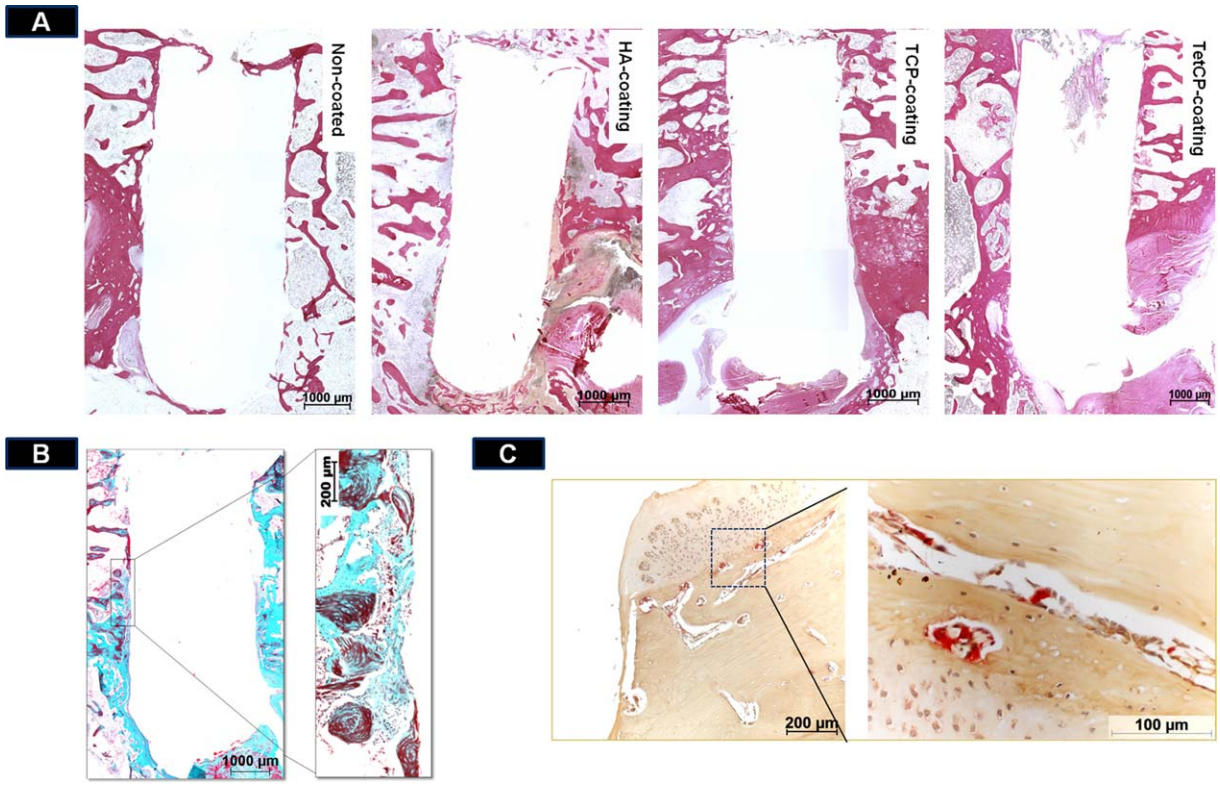

FIGURE 7. Histological sections after 6 weeks of implantation in the femoral condyle of rabbits: A: Elastica-van Gieson stain of the different experimental implants (non-coated, HAH, TCPH, and TTCPH). White area represents the original implant location; implants were removed for subsequent decalcification, paraffin-embedding and sectioning. B: Masson-Goldner stain at a higher magnification of the interface. C: Tartrate-resistant acid phosphatase positive staining at a higher magnification that shows the presence of osteoclast. [Color figure can be viewed in the online issue, which is available at wileyonlinelibrary.com.]

with different CaP target materials on (i) *in vitro* dissolution, and (ii) *in vivo* bone response. We hypothesized that CaP-based target materials would lead to coating-specific dissolution/precipitation behavior *in vitro* and bone response *in vivo*. This study showed that the initially deposited coatings all have a similar apatitic structure based on XRD and FTIR analyses. However, when tested *in vitro*, the experimental groups showed different dissolution/precipitation behavior. Furthermore, results from the *in vivo* test showed that despite similar BIC and peri-implant BV for all experimental implants, the presence of TRAP-positive staining in the peri-implant region suggests an apparent increase in bone remodeling around the implant surfaces with increasing coating dissolution (i.e., TTCP > TCP > HA).

In this study, sputtered coatings with specific CaP content and properties were obtained using various starting CaP targets with different stoichiometry (i.e., HA, α-TCP, and TTCP). Phase purity of these targets was confirmed by X-ray diffraction patterns. SEM examination showed that all as-sputtered and heat treated coatings had a homogenous and dense structure. XRD measurements revealed that all the as-sputtered coatings were amorphous. In accordance with previous studies, after an additional heat treatment, the XRD of all the sputtered coatings changed to a random apatite structure.[26–28] Ca/P ratios of all coatings were higher than initial Ca/P ratios of the corresponding target materials as demonstrated by additional ICP-OES measurements (Table I). The higher Ca/P ratio of these coatings can be explained by preferential sputtering of calcium in growing films,[27] and by the fact that orthophosphate ions are more volatile than calcium ions during sputtering and are pumped away before being deposited on the substrate.[3,27–29] In particular, TCPH had a higher Ca/P ratio than expected, which may be due to more orthophosphate ions in TCP than in HA or TTCP. Although several studies have examined the properties of HA and β-TCP sputtered coatings,[29–32] as far as the authors are aware, only one study has been published dealing with TTCP sputtered coatings.[19]

Solubility of the various types of coatings was investigated during *in vitro* incubation in SBF. Calcium and phosphate ion deposition and formation of a calcium phosphate layer when exposed to SBF are necessary to initiate the growth of bone-like apatite on biocompatible implants. Surface morphological differences were already observed for the TCPH and TTCPH coatings after two weeks of immersion indicating that precipitation had occurred. FTIR and XRD analyses revealed that the precipitate observed on the TCPH and TTCPH coatings was carbonate apatite, the amount of which increased with immersion time in SBF, while the HAH surface remained unchanged. Calcium and phosphate ions are released due to local surface dissolution of TCPH and TTCPH coatings, which supersaturates the SBF

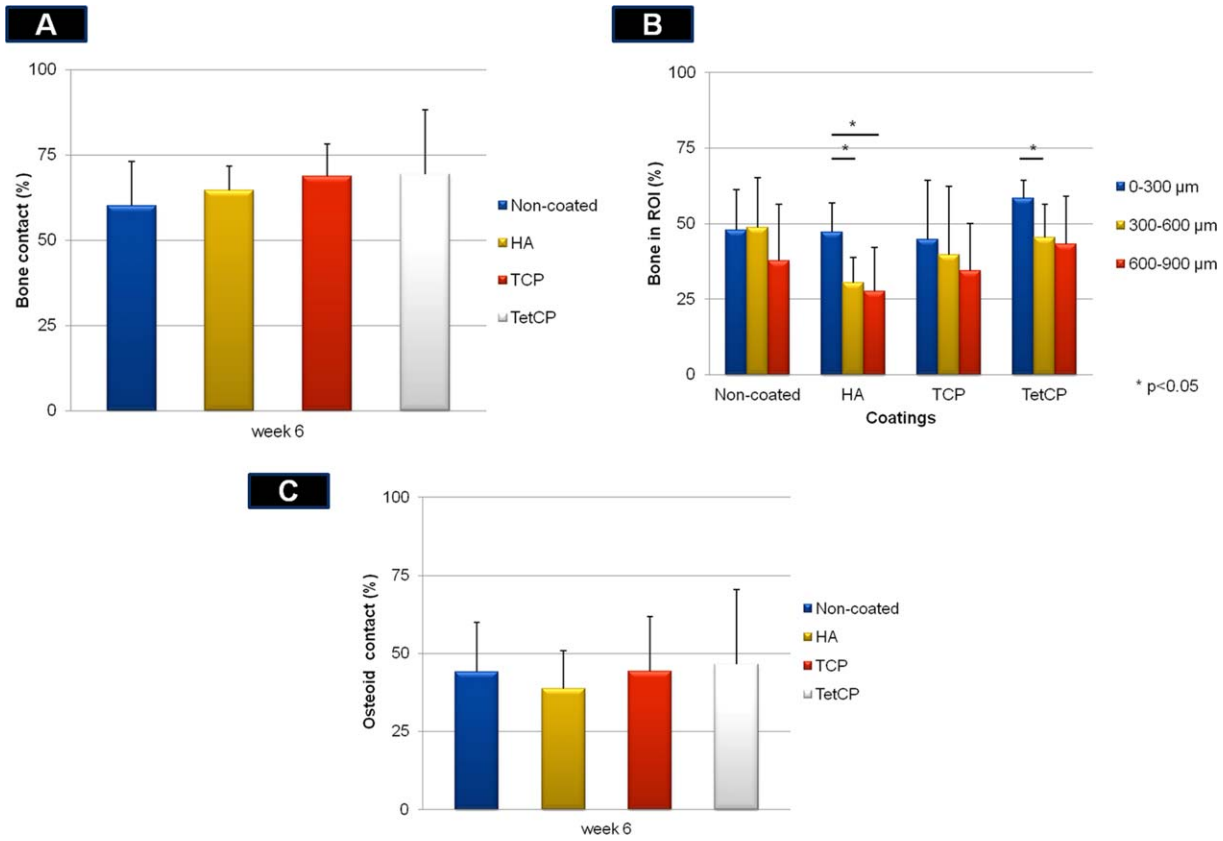

FIGURE 8. A: Results of histomorphometrical analysis of BIC percentage measurements for the different experimental implants (non-coated, HAH, TCPH, and TTCPH). B: Peri-implant BV percentage measurements for the different experimental implants (non-coated, HAH, TCPH, and TTCPH). *$p<0.05$. C: Results of histomorphometrical analysis of osteoid-implant contact measurements of non-coated, HAH, TCPH, and TTCPH. [Color figure can be viewed in the online issue, which is available at wileyonlinelibrary.com.]

promoting apatite nucleation and subsequently apatite precipitation. This phenomenon was not observed for the HAH coating, but several studies of CaP precipitation have demonstrated that the dissolution rate of α-TCP and TTCP is higher than that of hydroxyapatite.[33–35] After heat treatment, a different calcium phosphate phase could be expected for each CaP coating given the initial differences in Ca/P ratio of the target material. However, XRD measurements revealed that the heat treatment only induced a random apatite structural formation for all the as-sputtered coatings. It could be argued that the energy during heat treatment requires adjustment for individual CaP phases to achieve a more crystalline phase for each coating type in the present study. Also, the differences in coating dissolution are likely due to differences in atomic organization at the surface and the fraction of the as-sputtered CaP coating that was crystallized after the additional heat treatment.

The chemical composition of the coating surface is important, because the implant surface is the level at which the bone healing process starts. The femoral condyle rabbit model was chosen for the *in vivo* study because of its fast healing response and for comparison with other studies performed in our laboratory.[36] Previous work using RF magnetron sputtering to prepare bioactive CaP coatings showed accelerated implant stability by promoting rapid implant to bone fixation in different animal models, using rabbits,[36–38] goats,[32,39,40] dogs,[41–44] rats,[45] and primates.[46] A recent study showed favorable effects of CaP sputter-coatings on the bone implant interface in an osteoporotic rat model.[45] However, in this study, measurements of BIC 6 weeks after implantation in the rabbit model showed no significant differences between CaP coatings and non-coated implants. Previous studies on BIC found similar results using the same animal model, coating technique, and implantation time.[36,38] Furthermore, there is no difference in BIC between HA coatings and uncoated implants according to a recent review by Surmenev[3] on plasma-assisted CaP coatings fabrication methods. Only one study has shown higher BIC for crystalline HA coated implants 6 weeks after implantation in femoral bone in rabbits compared with non-

TABLE II. Percentage of Specimens with TRAP-Positive Presence at the Region Close to the Interface

Groups	TRAP-Positive Presence Percentage
Non-coated	17%
HAH	40%
TCPH	60%
TTCPH	75%

coated control implants.[37] To date, no studies have reported on TTCP-sputtered coatings upon *in vivo* implantation. The absence of an effect of the various CaP coatings on BIC can be due to the chosen implantation time. After 6 weeks of implantation, bone healing in a rabbit will be almost completed. Therefore, it is recommended to include shorter implantation times in future studies to allow for the observation of a possible effect during the initial stage of implant-bone healing. On the other hand, the results of this study showed differences in peri-implant BV formation in the inner 0–300 μm compared with middle 300–600 μm for the HAH and TTCPH coatings. Furthermore, there is an apparent increase in TRAP-positive staining percentage, which represents the presence of osteoclast-like cells, with decreasing coating stability. These results on BV formation and TRAP-positive staining indicate that variation in coating chemistry influences bone remodeling process directly adjacent to the implant surface.

Chemical composition and structural properties have been related with the osteoinductive capacity of CaP bulk ceramics in literature. The chemical composition is often the first coating parameter to be modified in studies. In a recent study, functionalized nanotopographic geometries on the surface of HA coated titanium implants were placed in heterotopic sites.[47] Induction of bone formation and regulation of gene products were observed to be functions of substrate topography, which dictated biological patterns.[47] Ripamonti et al.[47] conducted their study in heterotopic intramuscular sites, while CaP coatings were implanted in bone tissue in this study. The difference in implant location between this study and Ripamonti et al.[47] makes direct comparison inappropriate. However, the results of this study suggest that varying CaP stoichiometry gives different degrees of bone remodeling. In view of the results of Ripamonti et al.,[47] surface topography appears hierarchically superior to CaP stoichiometry for osteoinductive capacity of CaP-based ceramic coatings. However, supplementary chemical composition seems to represent a small but important approach to further influence peri-implant osteogenic processes.

CONCLUSION

This study has shown that differences in Ca/P ratio in sputter targets influence dissolution and precipitate formation of the resulting CaP coatings when tested *in vitro*. The *in vivo* study showed that neither peri-implant BV nor BIC were significantly affected in relation to different CaP coatings. However, the presence of TRAP-positive staining in the peri-implant region suggests increased bone remodeling around CaP-based coatings with lower stability (i.e., TTCPH > TCPH > HAH > non-coated controls). Future research should focus on combining critical surface parameters, e.g. coating composition and surface topography, to optimize surface properties for bone implants.

ACKNOWLEDGMENTS

The authors thank Mr. Vincent Cuijpers and Mr. Jan Mulder for their kind assistance in micro-CT 3D image reconstructions and statistical analyses, respectively.

REFERENCES

1. Dorozhkin SV, Epple M. Biological and medical significance of calcium phosphates. Angew Chem Int Ed Engl 2002;41:3130–3146.
2. Dorozhkin SV. Biphasic, triphasic and multiphasic calcium orthophosphates. Acta Biomater 2012;8:963–977.
3. Surmenev RA. A review of plasma-assisted methods for calcium phosphate-based coatings fabrication. Surf Coat Technol 2012; 206:2035–2056.
4. Yuan H, Fernandes H, Habibovic P, de Boer J, Barradas AM, de Ruiter A, Walsh WR, van Blitterswijk CA, de Bruijn JD. Osteoinductive ceramics as a synthetic alternative to autologous bone grafting. Proc Natl Acad Sci USA 2010;107:13614–13619.
5. Shadanbaz S, Dias GJ. Calcium phosphate coatings on magnesium alloys for biomedical applications: A review. Acta Biomater 2012;8:20–30.
6. Kim KH, Ramaswamy N. Electrochemical surface modification of titanium in dentistry. Dent Mater J 2009;28:20–36.
7. Voigt JD, Mosier M. Hydroxyapatite (HA) coating appears to be of benefit for implant durability of tibial components in primary total knee arthroplasty. Acta Orthop 2011;82:448–459.
8. Singh TP, Singh H, Singh H. Characterization of thermal sprayed hydroxyapatite coatings on some biomedical implant materials. J Appl Biomater Funct Mater 2012. DOI:10.5301/JABFM.2012.9267.
9. Suarez-Gonzalez D, Lee JS, Lan Levengood SK, Vanderby R, Jr., Murphy WL. Mineral coatings modulate beta-TCP stability and enable growth factor binding and release. Acta Biomater 2012;8: 1117–1124.
10. Roy M, Bandyopadhyay A, Bose S. In vitro antimicrobial and biological properties of laser assisted tricalcium phosphate coating. Mater Sci Eng C Mater Biol Appl 2009;29:1965–1968.
11. Tang R, Wu W, Haas M, Nancollas GH. Kinetics of dissolution of β-tricalcium phosphate. Langmuir 2001;17:3480–3485.
12. Moseke C, Gbureck U. Tetracalcium phosphate: Synthesis, properties and biomedical applications. Acta Biomater 2010;6:3815–3823.
13. de Bruijn JD, Bovell YP, van Blitterswijk CA. Structural arrangements at the interface between plasma sprayed calcium phosphates and bone. Biomaterials 1994;15:543–550.
14. Klein CP, Patka P, Wolke JG, de Blieck-Hogervorst JM, de Groot K. Long-term in vivo study of plasma-sprayed coatings on titanium alloys of tetracalcium phosphate, hydroxyapatite and alpha-tricalcium phosphate. Biomaterials 1994;15:146–150.
15. de Groot K, Geesink R, Klein CP, Serekian P. Plasma sprayed coatings of hydroxylapatite. J Biomed Mater Res 1987;21:1375–1381.
16. Sun L, Berndt CC, Gross KA, Kucuk A. Material fundamentals and clinical performance of plasma-sprayed hydroxyapatite coatings: A review. J Biomed Mater Res 2001;58:570–592.
17. Kurzweg H, Heimann RB, Troczynski T, Wayman ML. Development of plasma-sprayed bioceramic coatings with bond coats based on titania and zirconia. Biomaterials 1998;19:1507–1511.
18. Wolke JG, van Dijk K, Schaeken HG, de Groot K, Jansen JA. Study of the surface characteristics of magnetron-sputter calcium phosphate coatings. J Biomed Mater Res 1994;28:1477–1484.
19. Ozeki K, Fukui Y, Aoki H. Influence of the calcium phosphate content of the target on the phase composition and deposition rate of sputtered films. Appl Surf Sci 2007;253:5040–5044.
20. Jansen JA, Wolke JG, Swann S, Van der Waerden JP, de Groot K. Application of magnetron sputtering for producing ceramic coatings on implant materials. Clin Oral Implants Res 1993;4:28–34.
21. Shi JZ, Chen CZ, Yu HJ, Zhang SJ. Application of magnetron sputtering for producing bioactive ceramic coatings on implant materials. Bull Mater Sci 2008;31:877–884.
22. Yoshinari M, Hayakawa T, Wolke JG, Nemoto K, Jansen JA. Influence of rapid heating with infrared radiation on RF magnetron-sputtered calcium phosphate coatings. J Biomed Mater Res 1997; 37:60–67.
23. Kokubo T, Takadama H. How useful is SBF in predicting in vivo bone bioactivity? Biomaterials 2006;27:2907–2915.
24. van der Lubbe HB, Klein CP, de Groot K. A simple method for preparing thin (10 microM) histological sections of undecalcified plastic embedded bone with implants. Stain Technol 1988;63:171–176.

25. Piattelli A, Trisi P, Passi P, Piattelli M, Cordioli GP. Histochemical and confocal laser scanning microscopy study of the bone-titanium interface: An experimental study in rabbits. Biomaterials 1994;15: 194–200.
26. Thian ES, Huang J, Best SM, Barber ZH, Bonfield W. Silicon-substituted hydroxyapatite thin films: Effect of annealing temperature on coating stability and bioactivity. J Biomed Mater Res A 2006; 78:121–128.
27. Yang Y, Agrawal CM, Kim KH, Martin H, Schulz K, Bumgardner ID, Ong JL. Characterization and dissolution behavior of sputtered calcium phosphate coatings after different postdeposition heat treatment temperatures. J Oral Implantol 2003;29:270–277.
28. Yang Y, Kim KH, Mauli Agrawal C, Ong JL. Effect of post-deposition heating temperature and the presence of water vapor during heat treatment on crystallinity of calcium phosphate coatings. Biomaterials 2003;24:5131–5137.
29. Toque JA, Hamdi M, Ide-Ektessabi A, Sopyan I. Effect of the precossing parameters on the integrity of calcium phosphate coatings produced by RF-magnetron sputtering. Int J Modern Phys B 2009;23:5811–5818.
30. Ievlev VM, Kostyuchenko AV, Belonogov EK, Barinov SM. Hardness and the nature of microplasticity of hydroxyapatite. Inorg Mater 2013;49:416–422.
31. Feddes B, Wolke JG, Vredenberg AM, Jansen JA. Initial deposition of calcium phosphate ceramic on polyethylene and polydimethylsiloxane by rf magnetron sputtering deposition: The interface chemistry. Biomaterials 2004;25:633–639.
32. Wolke JG, de Groot K, Jansen JA. Subperiosteal implantation of various RF magnetron sputtered Ca-P coatings in goats. J Biomed Mater Res 1998;43:270–276.
33. Kim H, Camata RP, Vohra YK, Lacefield WR. Control of phase composition in hydroxyapatite/tetracalcium phosphate biphasic thin coatings for biomedical applications. J Mater Sci Mater Med 2005;16:961–966.
34. Klein CP, de Blieck-Hogervorst JM, Wolke JG, de Groot K. Studies of the solubility of different calcium phosphate ceramic particles in vitro. Biomaterials 1990;11:509–512.
35. Lu X, Leng Y. Theoretical analysis of calcium phosphate precipitation in simulated body fluid. Biomaterials 2005;26:1097–1108.
36. Hulshoff JE, van Dijk K, van der Waerden JP, Wolke JG, Kalk W, Jansen JA. Evaluation of plasma-spray and magnetron-sputter Ca-P-coated implants: An in vivo experiment using rabbits. J Biomed Mater Res 1996;31:329–337.
37. Mohammadi S, Esposito M, Hall J, Emanuelsson L, Krozer A, Thomsen P. Short-term bone response to titanium implants coated with thin radiofrequent magnetron-sputtered hydroxyapatite in rabbits. Clin Implant Dent Relat Res 2003;5:241–253.
38. Kyosuke Ueda YK, Narushima T, Goto T, Kurihara J, Nakagawa H, Kawamura H, Taira M. Calcium phosphate films with/without heat treatments fabricated using RF magnetron sputtering. J Biomech Sci Eng 2009;4:392–403.
39. Vercaigne S, Wolke JG, Naert I, Jansen JA. A histological evaluation of TiO2-gritblasted and Ca-P magnetron sputter coated implants placed into the trabecular bone of the goat: Part 2. Clin Oral Implants Res 2000;11:314–324.
40. Hulshoff JE, Jansen JA. Initial interfacial healing events around calcium phosphate (Ca-P) coated oral implants. Clin Oral Implants Res 1997;8:393–400.
41. Ueda K, Narushima T, Goto T, Taira M, Katsube T. Fabrication of calcium phosphate films for coating on titanium substrates heated up to 773 K by RF magnetron sputtering and their evaluations. Biomed Mater 2007;2:S160–S166.
42. Ong JL, Bessho K, Cavin R, Carnes DL. Bone response to radio frequency sputtered calcium phosphate implants and titanium implants in vivo. J Biomed Mater Res 2002;59:184–190.
43. Ozeki K, Yuhta T, Aoki H, Nishimura I, Fukui Y. Push-out strength of hydroxyapatite coated by sputtering technique in bone. Biomed Mater Eng 2001;11:63–68.
44. Ueda K, Narushima T, Goto T, Katsube T, Nakagawa H. Evaluation of calcium phosphate coating films on titanium fabricated using RF magnetron sputtering. Mater Trans 2007;48:307–312.
45. Alghamdi HS, Bosco R, van den Beucken JJ, Walboomers XF, Jansen JA. Osteogenicity of titanium implants coated with calcium phosphate or collagen type-I in osteoporotic rats. Biomaterials 2013;34:3747–3757.
46. Fugl A, Ulm C, Tangl S, Vasak C, Gruber R, Watzek G. Long-term effects of magnetron-sputtered calcium phosphate coating on osseointegration of dental implants in non-human primates. Clin Oral Implants Res 2009;20:183–188.
47. Ripamonti U, Roden LC, Renton LF. Osteoinductive hydroxyapatite-coated titanium implants. Biomaterials 2012;33:3813–3823.